Available online at www.sciencedirect.com
SCIENCE DIRECT
Marine Chemistry 100 (2006) 53–65
MARINE CHEMISTRY
www.elsevier.com/locate/marchem

Determination of the rate constants for the carbon dioxide to bicarbonate inter-conversion in pH-buffered seawater systems

K.G. Schulz [a,*], U. Riebesell [a], B. Rost [b], S. Thoms [b], R.E. Zeebe [c]

[a] Leibniz Institute for Marine Sciences, Düsternbrooker Weg 20, 24105 Kiel, Germany
[b] Alfred Wegener Institute for Polar and Marine Research, P.O. Box 12016, 27515 Bremerhaven, Germany
[c] University of Hawaii at Manoa SOEST Department of Oceanography 1000 Pope Road, MSB, 504 Honolulu, HI 96822, USA

Received 20 April 2005; received in revised form 11 November 2005; accepted 11 November 2005
Available online 4 January 2006

Abstract

Experimental setups to study modes of inorganic carbon acquisition and fixation rates by marine phytoplankton commonly make use of so-called disequilibrium techniques. The chemical or isotopic disequilibrium, either caused by phytoplankton cells taking up inorganic carbon or by a small disturbance of the isotopic equilibrium in the carbonate system, requires to account for the relatively slow chemical interconversion of carbon dioxide (CO_2) to bicarbonate (HCO_3^-) in seawater. Because in such experiments a constant pH is a prerequisite, pH buffers are generally used. However, a possible influence of such buffers on the kinetics of the carbonate system has hitherto not been investigated. Here, a model of the carbonate system in seawater is employed to show how pH buffers are operating. Furthermore, a new approach is presented to determine the rate constants, k_+ and k_-, for the conversion reaction of CO_2 to HCO_3^- and vice versa, by means of membrane inlet mass spectrometry (MIMS). For the two pH buffers tested (HEPES and BICINE) it is shown that measured rate constants are in good agreement with calculated values for k_+ and k_- in a pH range of 7 to 8.5 and at temperatures from 10 to 25 °C.
© 2005 Elsevier B.V. All rights reserved.

Keywords: CO_2 HCO_3^- interconversion; Rate constants; pH buffer; Disequilibrium; MIMS

1. Introduction

In the last 200 years, starting with the industrial revolution, the ocean has taken up ~50% of the carbon dioxide (CO_2) emitted by mankind's consumption of fossil fuels. The projected doubling of current atmospheric CO_2 around the year 2100 (Houghton et al., 1995) and its continuing oceanic uptake will give rise to a 60% increase in hydrogen ion concentration in the surface ocean (Sabine et al., 2004). This ocean acidification also involves a redistribution in the dissolved inorganic carbon (DIC) pool, increasing CO_2 and bicarbonate (HCO_3^-) at the expense of carbonate ion (CO_3^{2-}) concentrations. It has been shown, both in experimental and in modelling studies, that mechanisms and efficiencies of inorganic carbon acquisition by marine phytoplankton, which is responsible for about half of global net primary production (Field et al., 1998), are sensitive to the availability of CO_2 in seawater (Burkhardt et al., 2001; Rost et al., 2003; Thoms

* Corresponding author. Tel.: +49 431 600 4510; fax: +49 431 600 1515.
E-mail addresses: kschulz@ifm-geomar.de (K.G. Schulz), uriebesell@ifm-geomar.de (U. Riebesell), brost@awi-bremerhaven.de (B. Rost), sthoms@awi-bremerhaven.de (S. Thoms), zeebe@hawaii.edu (R.E. Zeebe).

0304-4203/$ - see front matter © 2005 Elsevier B.V. All rights reserved.
doi:10.1016/j.marchem.2005.11.001

et al., 2001). Moreover, these can differ greatly between various groups of phytoplankton species (Rost et al., 2003, in press). The consequences of future DIC redistribution for species composition and inorganic carbon fixation, however, are largely unknown. Assessment of these potential changes includes studies on mechanisms and efficiencies of inorganic carbon acquisition by different phytoplankton groups, making use of so-called disequilibrium techniques. While the mass spectrometric approach measures the disequilibrium caused by photosynthetic uptake of inorganic carbon (Badger et al., 1994), the ^{14}C disequilibrium technique monitors inorganic carbon fixation upon a small disturbance in the isotopic equilibrium of the carbonate system (Cooper et al., 1969; Espie and Colman, 1986). Both methods require exact knowledge of the response of the carbonate system to the disequilibrium employed, i.e., the kinetic rate constants for the chemical interconversion between CO_2 and HCO_3^-. Here we present a method for the exact determination of these rate constants by means of membrane inlet mass spectrometry (MIMS) and compare it with an approach described previously. Furthermore, adopting a model of the carbonate system in seawater, we explore the validity of the assumptions associated with these two approaches.

2. Methods

2.1. The experimental setup

All measurements were performed in artificial seawater following the recipe of Roy et al. (1993) without addition of DIC. The artificial seawater was divided into two batches to which BICINE or HEPES buffer were added yielding final concentrations of 50 μmol kg^{-1}. Sub-samples were taken and their pH was adjusted at room temperature to values of approximately 7.0, 8.0 and 8.4 by addition of NaOH. Subsamples were then incubated at temperatures of 11, 17 and 26 °C. For a measurement 8 ml of a seawater sample was filled into a thermostated cuvette (set to the desired temperature), attached to a sectorfield multicollector mass spectrometer (Isoprime; GV Instruments, England) via a gas permeable membrane (0.01 mm PTFE) inlet system. The area for gas exchange via the inlet system was about 24 mm^2 and was located at the bottom of the cuvette. The cuvette was closed without headspace to prevent significant gas exchange between atmosphere and water, and was equipped with a magnetic stirring rod to enhance mixing. Manipulations of the carbonate system in the cuvette were carried out via a tiny hole drilled into the stopper. Changes in concentrations of $^{12}CO_2$ and $^{13}CO_2$, the only species of dissolved inorganic carbon (DIC) which are measured directly by the membrane inlet mass spectrometer (MIMS), upon disturbance of the seawater carbonate system were monitored continuously with a resolution of 0.1 s (carbon species without ^{13}C or ^{12}C notation will refer to the sum of both). The MIMS was calibrated for $[CO_2]$ by injections of known amounts of $NaH^{12}CO_3$ (~ 99% ^{12}C) and $NaH^{13}CO_3$ (~ 99% ^{13}C) solutions (10 mmol kg^{-1}) into the cuvette filled with 8 ml of 0.2 M HCl. As in such acidic solution DIC is only present as CO_2 the measured CO_2 recording can be directly converted into concentration. The CO_2 baseline was determined by injection of 20 μl of 10 M NaOH. This increased seawater pH to values at which $[CO_2]$ is practically zero. As a single measurement did not exceed 10 min CO_2 consumption by the mass spectrometer through the membrane inlet system was negligible.

Special care was taken in determining the pH in all buffered seawater solutions. Known amounts (40 μl) of a $NaHCO_3$ solution (100 mmol kg^{-1}) were added to these and subsequent equilibration in the CO_2 signal was monitored. The $[CO_2]$ calibration of the MIMS was used to determine the DIC to CO_2 ratio (R_C) in equilibrium. Together with the dissociation constants of carbonic acid of Roy et al. (1993), the pH was calculated on the total scale (for details see Zeebe and Wolf-Gladrow (2001)). The pH of the seawater buffered with HEPES or BICINE remained rather constant (± 0.05 units) upon $NaHCO_3$ addition which was checked independently with a pH meter.

Previously, similar experimental setups were used for estimation of the rate constants for the CO_2 to HCO_3^- interconversion (e.g., Badger et al., 1994; Sültemeyer et al., 1995). Basically, CO_2 evolution was measured after injection of known amounts of a K_2CO_3 solution (100 mmol kg^{-1}) into DIC free seawater medium. In the alkaline K_2CO_3 solution (pH ~11) DIC is only present as CO_3^{2-} and HCO_3^- while CO_2 is practically zero. Hence, injection of such solution will result in a net conversion of CO_3^{2-} to HCO_3^- and finally to CO_2 in any seawater sample buffered at a pH lower than that of the K_2CO_3 solution. From the initial slope of the CO_2 evolution signal, monitored with the MIMS, the rate constants were then estimated. However, three assumptions regarding this procedure remain to be tested. First, the pH buffer is able to keep the pH constant on time scales of seconds recorded by the MIMS. Second, on these time scales the CO_3^{2-} and HCO_3^- pools are always in chemical equilibrium. And third, the initial reaction is dominated by the HCO_3^- to CO_2 conversion, so that the back-reaction can safely be

ignored. The first two assumptions are discussed in Sections 3.1, 3.2 and 3.4. As the third clearly poses a limitation a new method was developed which uses not only the initial slope but rather the entire CO_2 evolution curve, allowing explicitly for the back-reaction to take place. Practically, this is achieved by nonlinearly fitting a suitable equation to the measured CO_2 evolution curve leading to determination of the rate constants. However, these can also be assessed by adding known amounts of a solution in which DIC is mainly present in the form of CO_2. Such a solution was prepared by bubbling the artificial seawater described above with CO_2 at the desired temperature. Injection of this solution with a pH ~3.8 in any seawater sample, buffered at a pH higher than that, will result in a net conversion of CO_2 to HCO_3^-. Therefore, the MIMS will monitor a decrease in the CO_2 signal, the opposite reaction compared to K_2CO_3 addition.

2.2. The chemical background and the development of the fitting equations for addition of K_2CO_3 and CO_2 solutions

Inorganic carbon in aqueous solutions is predominantly present in three forms, CO_2(aq), HCO_3^- and CO_3^{2-}. The fourth compound, true carbonic acid (H_2CO_3), constitutes less than 0.1‰ of the total dissolved inorganic carbon (DIC) and is therefore generally added to the CO_2(aq) pool, defining CO_2 as the sum of CO_2(aq) and H_2CO_3. Then, this system is characterized by two reactions. The first can be described as the relation between the CO_2 and HCO_3^- pools in equilibrium

$$K_1^* = \frac{[H^+][HCO_3^-]}{[CO_2]} = \frac{k_+}{k_-} \quad (1)$$

with K_1^* being the stoichiometric equilibrium constant and k_+ and k_- referring to the rate constants for the overall reaction of CO_2 to HCO_3^- and vice versa, respectively. The kinetics between these pools can then be described as

$$H_2O + CO_2 \underset{k_-}{\overset{k_+}{\rightleftharpoons}} HCO_3^- + H^+. \quad (2)$$

This overall reaction comprises several reaction pathways for the CO_2 to HCO_3^- interconversion, given by Eqs. (17) and (18). Please note that in Eq. (17) the reaction pathway via H_2CO_3 is implicity included (see Appendix). Rate constants are dependent on temperature and salinity, but the actual rate at which equilibrium will be restored after a disturbance in one pool also depends on pH (note the $[H^+]$ in Eq. (1)). The second reaction in the carbonate system, the one between HCO_3^- and CO_3^{2-}, is virtually instantaneous compared to the reaction in Eq. (2), as it involves just protonation and deprotonation steps (see Section 3.4 for details).

The ratio of [DIC] to CO_2 in equilibrium ($[CO_2]_{eq}$) as measured with the MIMS is defined as

$$R_C = \frac{[DIC]}{[CO_2]_{eq}}. \quad (3)$$

From Eq. (2) follows that changes in $[CO_2]$ can be described as:

$$\frac{d[CO_2]}{dt} = +k_-[H^+][HCO_3^-] - k_+[CO_2] \quad (4)$$

this is a safe assumption on a time scale of seconds, as the HCO_3^- and CO_3^{2-} pools will be in equilibrium by the comparatively rapid reactions between them (see Section 3.4 for details). As $[CO_2]$ is the only parameter which can be monitored online by the MIMS, ([DIC]–$[CO_2]$–$[CO_3^{2-}]$) is substituted for $[HCO_3^-]$. Now, the only unknown in a redistribution of the carbonate species is $[CO_3^{2-}]$. Note that [DIC] is always conserved, even when the relative contribution of the three carbonate species changes. If the pH buffer (HEPES, or BICINE) is able to keep the pH constant (this assumption will be investigated with a model described in Section 2.4), $[CO_3^{2-}]$ can be described as a constant fraction f of $[HCO_3^-]$, yielding $[CO_3^{2-}] = f[HCO_3^-]$ (see 3.4 for details). Combining the last two equations gives

$$[HCO_3^-] = \frac{[DIC] - [CO_2]}{(1+f)}. \quad (5)$$

By substituting $[HCO_3^-]$ from Eq. (5) into Eq. (4) it follows that

$$\frac{d[CO_2]}{dt} = +k_-[H^+]\frac{[DIC] - [CO_2]}{(1+f)} - k_+[CO_2]. \quad (6)$$

Rearrangement with $\alpha = 1/(1+f)$ yields

$$\frac{d[CO_2]}{dt} = -(\alpha k_-[H^+] + k_+)[CO_2] + \alpha k_-[H^+][DIC]. \quad (7)$$

From here on, the paths for describing the CO_2 evolution curve upon addition of a K_2CO_3 or CO_2 solution split up. First, K_2CO_3 addition is considered. As right after the injection of a K_2CO_3 solution the reaction involving k_- will be the dominant one, k_+ is expressed in terms of k_- as described by equilibrium conditions in Eq. (1). Additionally, for convenience, the rate constant k_- is combined with $[H^+]$ giving $k_-^* = k_-[H^+]$ (note

that this is justified by the assumption that the pH is constant).

$$\frac{k_+}{k_-^*} = \frac{\left[HCO_3^-\right]_{eq}}{[CO_2]_{eq}} = \frac{\alpha\left([DIC] - [CO_2]_{eq}\right)}{[CO_2]_{eq}} = \alpha(R_C - 1) \quad (8)$$

Substituting now k_+ in Eq. (7) it follows that

$$\frac{d[CO_2]}{dt} = -\alpha R_C k_-^* [CO_2] + \alpha k_-^* [DIC]. \quad (9)$$

The general solution of the homogeneous version of Eq. (9) (i.e., [DIC]=0) is

$$[CO_2](t) = A\exp\left(-\alpha R_C k_-^* t\right) \quad (10)$$

where A is a constant to be determined from the initial conditions. One arbitrary solution of the non-homogeneous equation is (this can usually be found by assuming $[CO_2](t)$=constant):

$$[CO_2](t) = \frac{1}{R_C}[DIC]. \quad (11)$$

Hence, the general solution of the non-homogeneous equation is:

$$[CO_2](t) = A\exp\left(-\alpha R_C k_-^* t\right) + \frac{1}{R_C}[DIC] \quad (12)$$

Now A has to be determined from the initial condition $[CO_2](t=0)=[CO_2]_0=A+\alpha[DIC]/\alpha R_C$. And thus

$$A = [CO_2]_0 - \frac{1}{R_C}[DIC] \quad (13)$$

which leads to

$$[CO_2](t) = \left\{[CO_2]_0 - \frac{1}{R_C}[DIC]\right\}\exp\left(-\alpha R_C k_-^* t\right) + \frac{1}{R_C}[DIC] \quad (14)$$

with $[CO_2]_0$ being the initial $[CO_2]$ prior to addition of a K_2CO_3 solution. The constant R_C is determined with the MIMS as described above, and f can be calculated using the second dissociation constants of carbonic acid given by Roy et al. (1993). Then, Eq. (14) is fitted for k_-^* in a least square procedure to the observed CO_2 evolution data upon K_2CO_3 addition. From equilibrium conditions described in Eq. (1), k_+ can then be calculated as

$$k_+ = \frac{K_1^* k_-^*}{[H^+]} \quad (15)$$

with $k_- = k_-^* / [H^+]$.

In principle, Eq. (14) is equally suitable for CO_2 addition. However, the first dominant reaction will be the conversion of CO_2 to HCO_3^-. Hence, k_+ is substituted for k_- in Eq. (7). Further rearrangement and solving of the resulting differential equation gives

$$[CO_2](t) = \left\{[CO_2]_0 - \frac{1}{R_C}[DIC]\right\}\exp(-\gamma k_+ t) + \frac{1}{R_C}[DIC] \quad (16)$$

with $\gamma = R_C/(R_C - 1)$.

2.3. The fitting procedure

Fitting of Eqs. (14) and (16) to the observed CO_2 evolution curve ($^{12}CO_2 + {}^{13}CO_2$) upon addition of a K_2CO_3 or CO_2 solution is achieved by a least square minimization using the Levenberg–Marquardt method (Moré, 1977), yielding k_- or k_+, respectively. There are, however, always two processes influencing the CO_2 evolution curve in the first couple of seconds following a disturbance in the carbonate system, i.e., changes in the gas flow through the membrane and mixing of the DIC addition in the cuvette. This is accounted for by discarding the first couple of seconds and starting the fitting procedure from the inflection point (see Fig. 1).

As stated earlier, a crucial prerequisite for the fitting equations is that the pH of the seawater is kept constant by the pH buffer throughout the measurement. Therefore, in the next section a model of the carbonate system in seawater is described to test this assumption.

2.4. The model of the carbonate system in seawater

A model similar to that of Zeebe and Wolf-Gladrow (2001) was developed, including all important reactions of the carbonate system in seawater. Additionally, a parameterization for the kinetics of different pH-buffers was added. Boron species, important constituents in natural seawater, are excluded because they are not contained in the artificial seawater used. The following reactions are considered (the letter A denotes a proton acceptor, i.e., a pH buffer).

$$CO_2 + H_2O \underset{k_{-1}}{\overset{k_{+1}}{\rightleftharpoons}} HCO_3^- + H^+ \quad (17)$$

$$CO_2 + OH^- \underset{k_{-4}}{\overset{k_{+4}}{\rightleftharpoons}} HCO_3^- \quad (18)$$

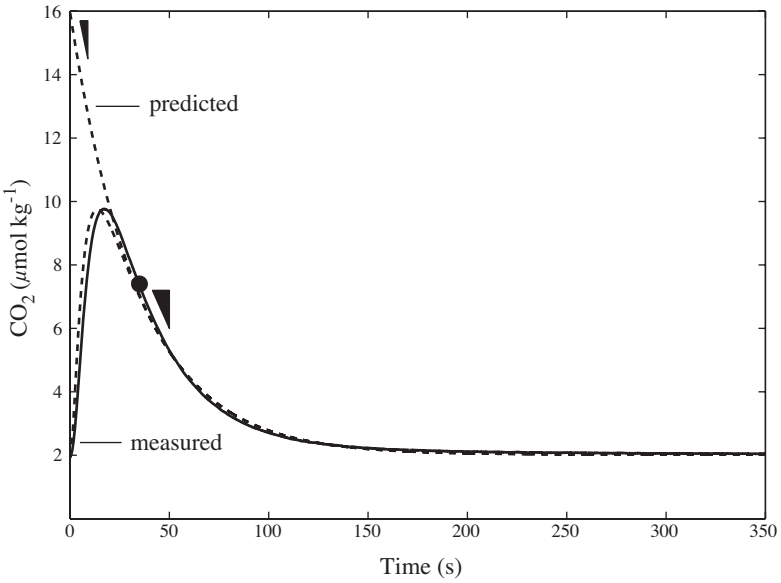

Fig. 1. Example for the measurement of the CO_2 ($^{12}CO_2 + {}^{13}CO_2$) evolution curve as monitored with the MIMS upon an addition of ~14 μmol kg^{-1} CO_2, and the curve fitting procedure. The solid line depicts the change in [CO_2] as measured by the MIMS and the dashed line the CO_2 evolution curve as predicted by Eq. (16) after the fitting procedure described in Section 2.3. The dot marks the inflection point at which the fitting to the solid line is started. The dashed line increasing constantly prior to that point is the theoretical decline in [CO_2] (Eq. (16)) which would be observed in an ideal situation, i.e. right at time zero, the injected CO_2 is mixed homogeneously in the cuvette and detected instantly by the MIMS. To illustrate these processes the theoretical CO_2 evolution curve has been modified by multiplication with two exponential terms representing mixing and changing gas flow through the membrane (dashed line starting at the initial [CO_2] at time zero). This theoretical CO_2 evolution curve resembles the measured very well and demonstrates that the fitting procedure after the inflection point is not biased by mixing and changing gas flow through the membrane. The two solid triangles next to the CO_2 evolution curves illustrate the respective slopes at time zero and after the inflection point, at which the back-reaction from HCO_3^- to CO_2 is much higher and [CO_2] is much lower, resulting in a shallower slope. In the case shown, the temperature was 17 °C, the seawater pH was ~8 and the pH buffer used was HEPES.

$$CO_3^{2-} + H^+ \underset{k_{-5}^{H^+}}{\overset{k_{+5}^{H^+}}{\rightleftharpoons}} HCO_3^- \tag{19}$$

$$HCO_3^- + OH^- \underset{k_{-5}^{OH^-}}{\overset{k_{+5}^{OH^-}}{\rightleftharpoons}} CO_3^{2-} + H_2O \tag{20}$$

$$H_2O \underset{k_{-6}}{\overset{k_{+6}}{\rightleftharpoons}} H^+ + OH^- \tag{21}$$

$$AH \underset{k_{-a}}{\overset{k_{+a}}{\rightleftharpoons}} A^- + H^+ \tag{22}$$

It is noted that, what is referred to as k_+ or k_- in Eq. (2) must not be confused with k_{+1} or k_{-1} in Eq. (17). The former are the rate constants for the overall reactions between the CO_2 and HCO_3^- pools in this coupled chemical system. The values for the different reaction rate constants are given in Table 1. The set of differential equations therefore reads

$$\frac{d[CO_2]}{dt} = +(k_{-1}[H^+] + k_{-4})[HCO_3^-] - (k_{+1} + k_{+4}[OH^-])[CO_2] \tag{23}$$

$$\frac{d[HCO_3^-]}{dt} = +(k_{+1} + k_{+4}[OH^-])[CO_2] - (k_{-1}[H^+] + k_{-4})[HCO_3^-] + \left(k_{+5}^{H^+}[H^+] + k_{+5}^{OH^-}\right)[CO_3^{2-}] - \left(k_{-5}^{H^+} + k_{+5}^{OH^-}[OH^-]\right)[HCO_3^-] \tag{24}$$

$$\frac{d[CO_3^{2-}]}{dt} = +\left(k_{-5}^{H^+} + k_{+5}^{OH^-}[OH^-]\right)[HCO_3^-] - \left(k_{+5}^{H^+}[H^+] + k_{-5}^{OH^-}\right)[CO_3^{2-}] \tag{25}$$

$$\frac{d[H^+]}{dt} = +k_{+1}[CO_2] - k_{-1}[H^+][HCO_3^-] + k_{-5}^{H^+}[HCO_3^-] - k_{+5}^{H^+}[H^+][CO_3^{2-}] + k_{+6} + k_{-6}[H^+][OH^-] + k_{+a}[AH] - k_{-a}[H^+][A^-] \tag{26}$$

Table 1
Rate constants and their respective check values used in this study

Rate constant	Check value T=298.15 K, S=35	Dependence on T and S	Reference
k_{+1}	3.71×10^{-2} s^{-1}	exp (1246.98 − 6.19 × 10^4/T − 183.0 ln (T))	1
k_{-1}	2.67×10^{4} kg mol^{-1} s^{-1}	k_{+1}/K_1^*	Calculated
k_{+4}	2.23×10^{3} kg mol^{-1} s^{-1}	A_4 exp (−90,166.83/(RT))/K_W^*	Refitted from 1
k_{-4}	9.71×10^{-5} s^{-1}	$k_{+4}\times K_W^*/K_1^*$	Calculated
$k_{+5}^{H^+}$	5.0×10^{10} kg mol^{-1} s^{-1}	None	2
$k_{-5}^{H^+}$	59.44 s^{-1}	$k_{+5}^{H^+}\times K_2^*$	Calculated
k_{+5}^{OH-}	6.0×10^{9} kg mol^{-1} s^{-1}	None	2
k_{-5}^{OH-}	3.06×10^{5} s^{-1}	$k_{-5}^{OH-}\times K_W^*/K_2^*$	Calculated
k_{+6}	1.40×10^{-3} mol kg^{-1} s^{-1}	None	2
k_{-6}	2.31×10^{-10} kg mol^{-1} s^{-1}	k_{+6}/K_W^*	Calculated
k_{+a}	s^{-1}	$k_{-a}\times10^{-pK_A}$	Calculated
k_{-a}	kg mol^{-1} s^{-1}	$k_{+5}^{H^+}/f_a$	Varied

Ref. 1 refers to the work of Johnson (1982), while Ref. 2 refers to the work of Eigen (1964) (see Zeebe and Wolf-Gladrow (2001), p. 105 for a detailed discussion). k_{+4} has been refitted in this study, with A_4=499,002.24 × exp(4.2986 × 10^{-4} S^2 +5.75499 × 10^{-5} S), with S representing salinity because otherwise measured and calculated values for k_+ did not match well, especially at high temperature. pK_A denotes the pK_A value of the pH buffer used, i.e. HEPES: pK=7.94 − 0.014 × (T − 273.15) and BICINE: pK=8.82 − 0.018 × (T − 273.15) after Good et al. (1966), with T representing temperature in Kelvin. These are values extrapolated to zero ionic strength (see Beynon and Easterby (1996) for details). In the calculations, however, they have been adjusted to the correct ionic strength with the Davies approximation (Davies, 1962). Rate constants for the pH buffer were varied by applying a factor f_a to k_{-a}. R denotes the universal gas constant of 8.31451 J/mol, K_W^* the equilibrium constant for the ion product of water calculated after DOE (1994), and K_1^* and K_2^* the first and second dissociation constants of carbonic acid calculated according to Roy et al. (1993). The corresponding reactions for the different rate constants are listed in Eqs. (17)–(22).

$$\frac{d[OH^-]}{dt} = +k_{-4}[HCO_3^-] - k_{+4}[OH^-][CO_2] - k_{+5}^{OH^-}[OH^-][HCO_3^-] + k_{-5}^{OH^-}[CO_3^{2-}] + k_{+6} + k_{-6}[H^+][OH^-] \quad (27)$$

$$\frac{d[AH]}{dt} = +k_{-a}[H^+][A^-] - k_{+a}[AH] \quad (28)$$

$$\frac{d[A^-]}{dt} = +k_{+a}[AH] - k_{-a}[H^+][A^-]. \quad (29)$$

This set of coupled differential equations was integrated numerically with the matlab 'ode15s' solver for 'stiff' problems (Shampine and Reichelt, 1997). These equations are called 'stiff' because the coupled system exhibits extremely different relaxation times (Zeebe et al., 1999).

3. pH-buffered seawater systems

Relaxation times of the carbonate system in pH-buffered seawater upon disturbance depends on the type and amplitude of the disturbance and most importantly on the kinetics of the pH buffer. However, rate constants for the protonation and deprotonation of widely used pH buffers are not available, and a general assumption is that the two reactions are almost instantaneous or at least sufficiently fast compared to other reactions that they can be ignored. In the following considerations, the rate constants for the pH buffer (i.e., its speed) were chosen to be about 100 times slower than the comparatively rapid CO_3^{2-} to HCO_3^- interconversion.

3.1. K_2CO_3 versus CO_2 addition

In Fig. 2 the response of the carbonate system upon addition of a K_2CO_3 solution to low-DIC (5 μmol kg^{-1}), pH-buffered seawater is shown (see caption of Fig. 2 for details). The amount of solution added was chosen to result in a 500 μmol kg^{-1} increase in DIC in the seawater sample. This setup resembles those previously used to determine k_- from the initial slope of CO_2 evolution (e.g., Badger et al., 1994; Sültemeyer et al., 1995). The re-equilibration in the carbonate system following the addition of a K_2CO_3 solution includes three characteristic time scales.

3.1.1. Time scale 10^{-10} to 10^{-5} s

Injection of a highly alkaline K_2CO_3 solution (pH ~11) into seawater of pH 8 significantly increases the OH^- concentration as illustrated by the drop in pOH, i.e., the negative common logarithm of [OH^-] in analogy to pH (Fig. 2E). This decrease in pOH leads to an immediate increase in pH (Fig. 2F) as the OH^- added consumes the H^+ present. Also shortly after injection of the K_2CO_3 solution, the conversion of the

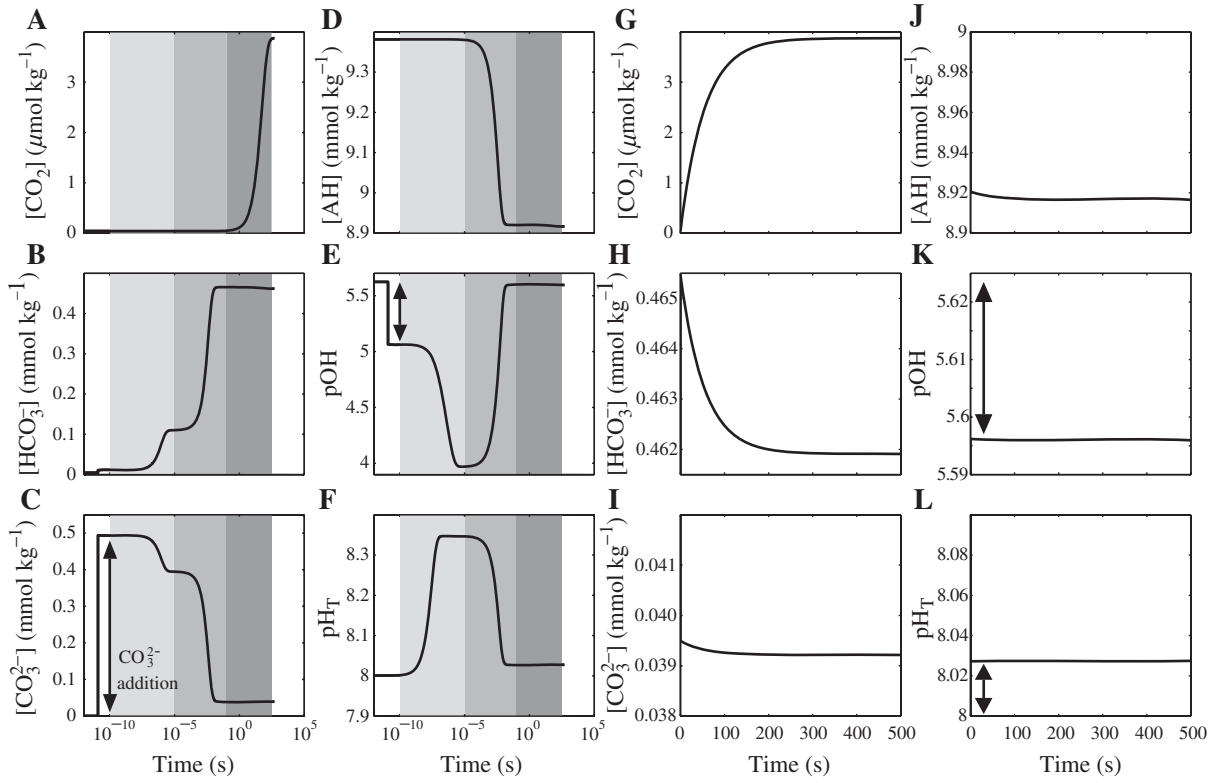

Fig. 2. Reaction kinetics in pH-buffered seawater upon addition of a K_2CO_3 solution (at t equals zero), leading to an increase in DIC of 500 μmol kg^{-1} in the seawater sample, as calculated by the numerical model described in Section 2.4. The pH buffer was set to 50 mM of HEPES, temperature to 15 °C, Salinity to 35, pH to 8.0, initial DIC to 5 μmol kg^{-1} and k_{-a} to $k_{+5}^{H^+}/100$. AH denotes the protonated form of the buffer. Illustrated in A–F are the changes of $[CO_2]$, $[HCO_3^-]$, $[CO_3^{2-}]$, [AH], pOH and pH (on the total scale) against time on a logarithmic scale, while in G–L the same reactions against time are shown on a linear scale. Grey shaded areas depict different timescales ranging from 10^{-10} to 10^{-5}, 10^{-5} to 10^{-1} and 10^{-1} to 400 seconds (light, intermediate and dark grey, respectively). The arrows denote changes from equilibrium due to the disturbance by the addition of a K_2CO_3 solution.

added CO_3^{2-} to HCO_3^- begins (Fig. 2B,C). In this reaction CO_3^{2-} combines with water giving HCO_3^- and OH^- (compare Eq. (20)) leading to a concomitant decrease in pOH (Fig. 2E). Why this reaction is dominating rather than the competing one, in which CO_3^{2-} combines with H^+ (Eq. (19)), can easily be understood by comparing the relevant terms, $k_{-5}^{OH^-}$ and $k_{+5}^{H^+}[H^+]$, in Eq. (25). As $k_{-5}^{OH^-}$ is about seven orders of magnitude larger than $k_{+5}^{H^+}[H^+]$, HCO_3^- is formed almost entirely by the combination of CO_3^{2-} with water. The decrease in pOH is not a mirror image of the increase in pH, indicating that the ion product of water (Eq. (21)) is not constant on this time scale. The reason is that the conversion of CO_3^{2-} to HCO_3^- is slightly faster than the combination reaction of H^+ and OH^-. Hence, the increase in pH lags behind the decrease in pOH. Furthermore, the protonated form of the pH buffer is already starting to release protons to compensate for the loss of H^+, dampening the increase in pH. This initial pH-buffering, however, is not visible in [AH] (Fig. 2D) as the amount of H^+ released by the protonated form of the buffer is about six orders of magnitude lower than the buffer's concentration (note that $[H^+]$ is in the nanomolar and [AH] in millimolar range). A temporary pH plateau of about 8.35 is reached after about 10^{-6} s. The height of this plateau depends on the rate constants of the pH buffer chosen. Increasing the rate constants increases the speed of the buffer and the temporary plateau will be closer to the final equilibrium value of about pH 8.0.

3.1.2. Time scale 10^{-5} to 10^{-1} s

The comparatively massive proton release by the protonated form of the buffer (Fig. 2D) yields to both, an increase of pOH (due to protonation of OH^-) and a decrease of pH (Fig. 2E,F). Hence, a second phase of CO_3 to HCO_3^- conversion is initiated (Fig. 2B,C). A temporary quasi steady-state between all these pools is established after about 10^{-2} s (Fig. 2B–F).

3.1.3. Time scale larger than 10^{-1} s

It is by now that the HCO_3^- and CO_2 pools start to re-equilibrate (Fig. 2A,B), owing to the slow interconversion rate. Again, the protonated form of the pH-buffer re-delivers the protons consumed by the conversion of HCO_3^- to CO_2 (Fig. 2D). However, as the pH-buffer was assumed orders of magnitude faster than the HCO_3^- to CO_2 conversion and the amount of protons released is small compared to those released due to the conversion of CO_3^{2-} to HCO_3^-, the pH and the pOH stay constant during this last phase of re-equilibration.

In this configuration (see caption of Fig. 2 for details), the pH-buffer was able to keep the pH constant on a time scale of seconds (Fig. 2L), which is a prerequisite for the fitting procedure. However, it is obvious that this depends on the actual rate constants assumed for the protonation/deprotonation reactions of the buffer (i.e., its speed). When adding a K_2CO_3 solution to a seawater system as described above, the pH buffer has to release far more protons consumed in the rapid conversion of CO_3^{2-} to HCO_3^- than from the slow reaction of HCO_3^- to CO_2.

This is opposite to addition of a CO_2 solution (Fig. 3), where the pH buffer has to accept more protons from the slow reaction. Again, there are three characteristic time scales for the re-equilibration.

3.1.4. Time scale 10^{-10} to 10^{-5} s

Injection of a CO_2 solution, yielding a final DIC concentration of 500 μmol kg^{-1}, in the buffered seawater (the preparation of such solution is described in Section 2.1), causes an initial drop in pH (Fig. 3F) as such a solution is highly acidic (pH ~3.8). Almost instantly the unprotonated form of the buffer starts to accept the H^+ added, leading to an increase in pH and [AH], the protonated form of the buffer (Fig. 3D). Please note that the total increase in pH from about 5.5 to 8.0 corresponds to a decrease in $[H^+]$ of about 3 μmol kg^{-1}. This is difficult to detect in the simultaneous increase in [AH] as, again, the buffer concentration is about four orders of magnitude higher than the amount of protons accepted. pH reaches a temporary plateau of about 8.0 already before 10^{-5} s. The time required to achieve this pH which is close to equilibrium conditions crucially

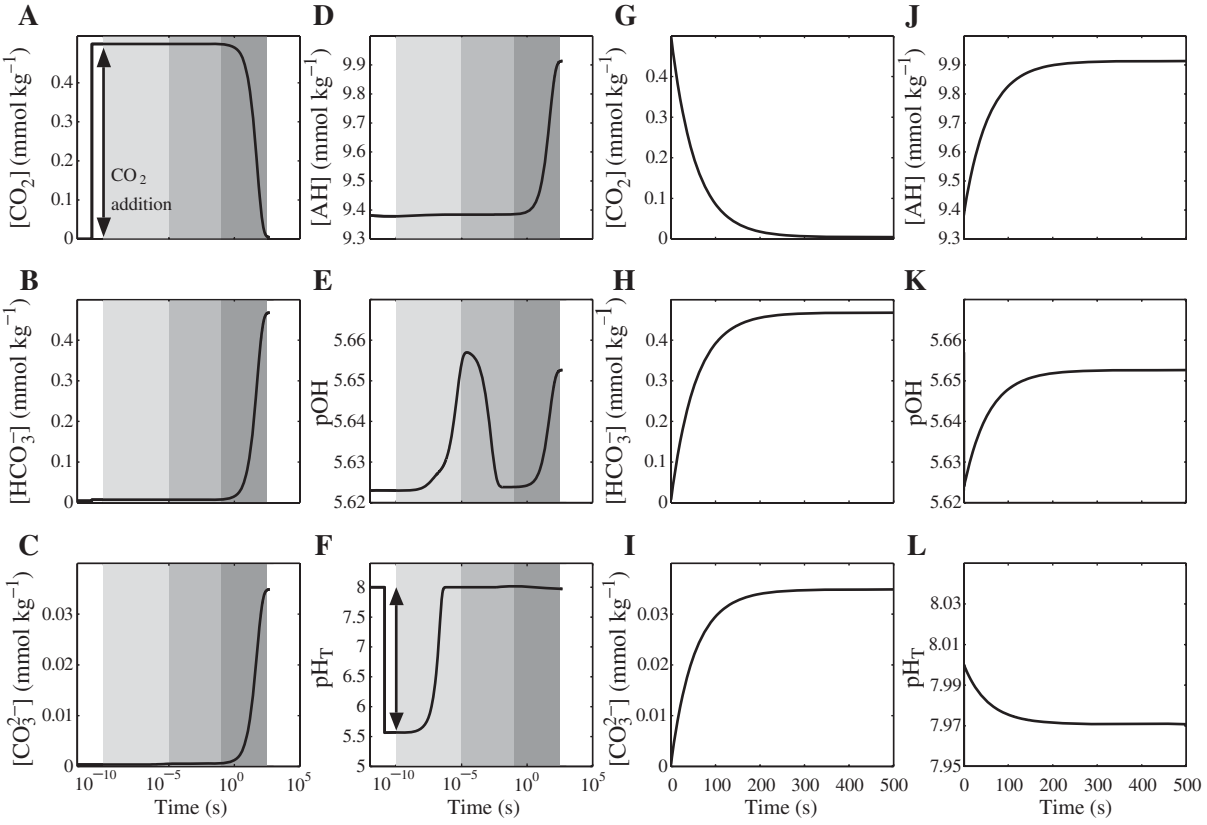

Fig. 3. Reaction kinetics in pH-buffered seawater upon addition of a CO_2 solution (at t equals zero), leading to an increase in DIC of 500 μmol kg^{-1} in the seawater sample, as calculated by the numerical model described in Section 2.4. For details see Fig. 2 caption.

depends on the rate constants of the buffer, i.e., its speed. Already shortly after the initial increase in pH there is an increase in pOH. This is partly caused by the combination of HCO_3^- with OH^- yielding CO_3^{2-} (Eq. (20)) because the injected CO_2 solution contains a small amount of HCO_3^- (~ 2.5 μmol kg^{-1}). Hence, part of the HCO_3^- (~0.2 μmol kg^{-1}) added convert to CO_3^{2-} resulting in the increase in pOH. Also responsible for the increase in pOH is the combination of the H^+ added with the OH^- present. However, the increase in pOH is not as pronounced as the increase in pH, indicating that the ion product of water on this time scale is not constant. This can be easily understood when comparing the equations competing for the H^+ added which are the formation of water with OH^- (Eq. (21)) and the combination with the unprotonated form of the buffer A^- (Eq. (22)). The relevant terms for these reactions given in Eq. (26) are $k_{-6}[OH^-]$ and $k_{-a}[A^-]$, respectively (note that $[H^+]$ is the same for both of them). As $k_{-a}[A^-]$, is about 200 times larger than $k_{-6}[OH^-]$ the increase in pH is dominated by the protonation of the buffer and not by OH^- consumption. Hence, the increase in pH is hardly reflected in pOH.

3.1.5. Time scale 10^{-5} to 10^{-1} s

The imbalance between the OH^- and H^+ pools start to re-equilibrate and the pOH drops to its initial value whereas the pH is kept constant by the buffer. Again, a temporary quasi steady-state between all these pools is established after about 10^{-2} s (Fig. 3B–F).

3.1.6. Time scale larger than 10^{-1} s

The slow conversion reaction of CO_2 to HCO_3^- is then initiated at about 10^{-1} s leading to a slight drop in pH and a concomitant increase in pOH compared to conditions prior to injection. And again, in this configuration (see caption of Fig. 3 for details) the buffer has been able to keep the pH very close to equilibrium values (Fig. 3L). Basically, if the protonation reaction of the buffer is faster than the conversion of CO_2 to HCO_3^- it can keep up with the release of protons by this process.

3.2. Influence of the pH buffer kinetics on changes in pH

As outlined above, a prerequisite for fitting of the CO_2 evolution curve upon addition of a K_2CO_3 or CO_2 solution (Figs. 2G and 3G, respectively) is that the pH can be considered constant. The rate constants for the protonation and deprotonation of certain pH buffers, however, are not known. Therefore, their influence on pH, following the addition of a K_2CO_3 or CO_2 solution, was investigated by varying the rate constants of the pH buffer in the seawater carbonate system model. More specifically, the time was determined after which the pH reached a constant value. For that, a critical threshold was introduced of 0.05 pH units which was the maximum pH drift from steady state conditions after injection of a K_2CO_3 or CO_2 solution, observed in all measurements. Calculated times to reach that threshold depend to a small degree on whether K_2CO_3 or CO_2 is added (Fig. 4A/B), but mostly on the pH of the seawater. The differences in pK values between HEPES and BICINE are negligible for the following considerations. The time to reach constant pH values is faster the lower the pH is regardless whether K_2CO_3 (Fig. 4A) or CO_2 (Fig. 4B) is added. When adding K_2CO_3 the protonated form of the pH buffer (AH) releases protons to compensate for the loss of H^+ consumed by the conversion of CO_3^{2-} to HCO_3^-. Hence, at low pH the initial concentration of AH is higher compared to high pH and the re-equilibration is faster. On the other hand, when adding CO_2 the unprotonated form of the buffer accepts the protons generated by the conversion of CO_2 to HCO_3^-. Hence at low pH, this protonation is enhanced by the increased $[H^+]$.

It seems that neither K_2CO_3 nor CO_2 addition bears any advantages for measuring the carbon dioxide to bicarbonate interconversion rates. However, the time to reach constant pH values is not only bound to buffer kinetics but also to the amplitude of the disturbance. Basically, the lower the amount of K_2CO_3 or CO_2 addition, the lower is the disequilibrium in $[H^+]$ the buffer has to cope with. Injecting a small amount of CO_2 and measuring its disappearance into the HCO_3^- and CO_3^{2-} pools is possible, while the same amount injected as K_2CO_3 will result in almost no detectable change in $[CO_2]$ (note that in seawater, with a pH ranging from 7–9, the dominant DIC form is HCO_3^- while the MIMS is only able to detect CO_2 and the two other DIC species have to be deduced). This is illustrated in Figs. 3A and 2A, where the change in $[CO_2]$ due to a 500 μmol kg^{-1} addition of CO_2 is about 500 μmol kg^{-1}, while the addition of 500 μmol kg^{-1} of K_2CO_3 results in a change in $[CO_2]$ of only about 4 μmol kg^{-1}. Therefore, it is feasible to work with much lower additions of CO_2 compared to K_2CO_3, and the influence of the buffer kinetics on the time to reach constant pH values is becoming less critical (when adding 15 μmol kg^{-1} of CO_2 instead of 500 μmol kg^{-1} (compare Fig. 4A) the pH is constant from the first second, regardless of seawater pH and buffer kinetics). Hence, the experiments were carried

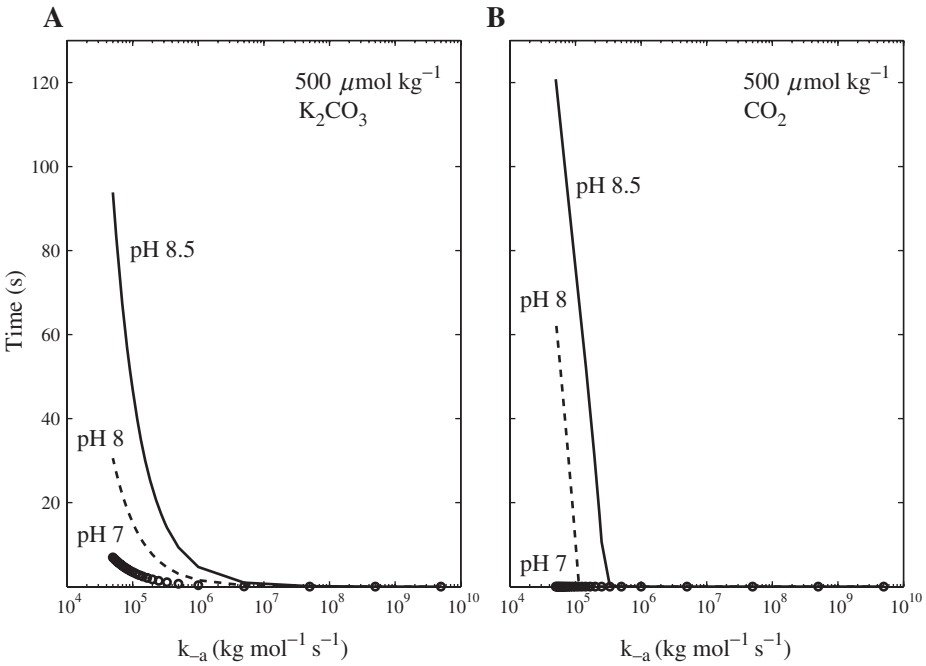

Fig. 4. Influence of the pH buffer kinetics on the pH re-equilibration time as predicted by the numerical model described in Section 2.4. The pH buffer was set to 50 mM of HEPES, temperature to 15 °C, salinity to 35, initial DIC to 5 μmol kg^{-1} and k_{-a} was varied. Solid lines are the results for a seawater pH of 8.5, dashed lines for a pH of 8.0 and circles for a pH of 7.0. Illustrated in A are the results upon an addition of 500 μmol kg^{-1} K_2CO_3 and in B the results upon an addition of 500 μmol kg^{-1} CO_2.

out with small amounts of CO_2 injected into seawater buffered at different pH values at certain temperatures, and the resulting decrease in $[CO_2]$ was monitored and fitted with Eq. (16) (Fig. 1).

3.3. The rate constants for CO_2 to HCO_3^- interconversion at different temperatures and pH

The k_+ values resulting from fitting the CO_2 evolution upon adding small amounts of CO_2 (yielding a final concentration of about 15 μmol kg^{-1}) to seawater buffered at pH values ranging from 7 to 9 and temperatures of 11, 16 and 26 °C are shown in Fig. 5. Also shown are calculated k_+ values from the second part of Eq. (23) with $k_+ = k_{+1} + k_{+4}[OH^-]$, the combination of reactions (17) and (18) (see Appendix for details). Because application of k_{+4} values, determined previously (Zeebe and Wolf-Gladrow, 2001) by fitting the original data from Johnson (1982), did not match the measurements (especially at 26 °C), k_{+4} has been refitted in this study (see Table 1 for details). Measured and calculated k_+ values are in good agreement in the pH range from 7 to 8.5, regardless whether HEPES or BICINE was used as pH buffer. This clearly indicates that both buffers are able to keep the pH constant under the experimental conditions tested. Above a pH of 8.5, however, correlation between measured and calculated values becomes less clear. One reason is that the error in pH determination with the MIMS increases with rising pH, because the contribution of CO_2 to DIC decreases. Hence, after additions of known amounts of $NaHCO_3$ to determine the DIC/CO_2 ratio, the change in $[CO_2]$ will get close to the noise in the CO_2 signal detected by the MIMS. Under these circumstances the pH cannot be calculated reliably anymore.

Furthermore, k_+ increases with rising temperature and pH (Fig. 5). High pH values correspond to increased $[OH^-]$ and therefore the reaction of $CO_2 + OH^- \rightarrow HCO_3^-$ is faster compared to low pH and k_+ is larger. Strictly speaking, the CO_2 evolution is characterized not by k_+ alone, but by γk_+ (see Eq. (16)). But at pH values above 7, $\gamma = R/(R-1)$ is almost equal to one and can be neglected (also compare solid line in Fig. 5 with Fig. 6A) From equilibrium conditions described in Eq. (1), it follows that $k_- = k_+ / K_1^*$.

From Fig. 1 it becomes evident that interpretation of initial CO_2 slopes recorded by the MIMS is difficult. This is due to the fact that in the first couple of seconds, following a disturbance, homogeneous mixing in the cuvette and changing gas fluxes through the membrane

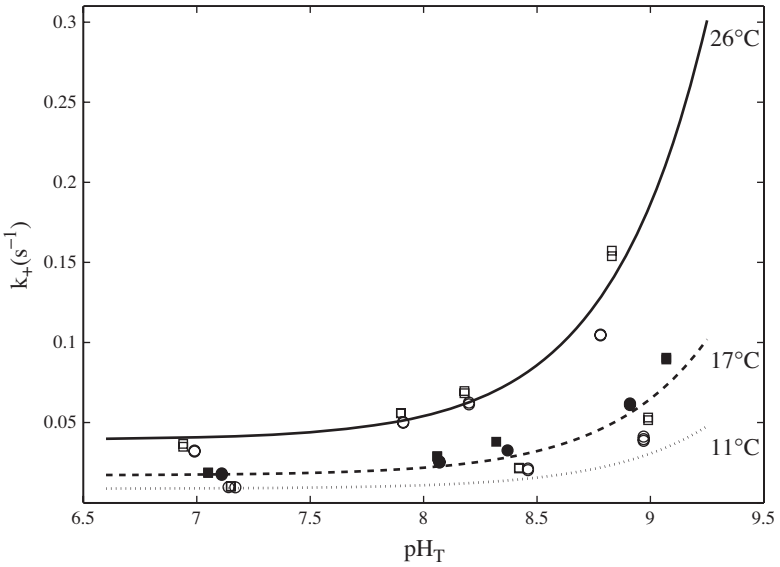

Fig. 5. Graphical illustration of the k_+ values determined with the fitting procedure shown in Fig. 1 and described in Section 2.3, measured by additions of ~15 μmol kg^{-1} CO_2 at different temperatures and seawater pH (total scale). Squares denote seawater buffered with 50 mM HEPES and circles seawater with 50 mM BICINE. The lines depict calculated k_+ with $k_+ = k_{+1} + k_{+4}[OH^-]$ (see Table 1 for details regarding the rate constants) at temperatures of 11 (dotted), 17 (dashed) and 26 °C (solid line).

mask the kinetics in the carbonate system. Thus, the initial slope of the CO_2 evolution curve (defined as the maximum slope) is always shallower than the slope that would be observed in an ideal setup. This can only be accounted for by fitting the CO_2 signal from the inflection point to a suitable equation, which explicitly incorporates the forward and backward reactions between the CO_2 and HCO_3^- pools. Hence, determination of k_- from the initial slope as proposed previously underestimates k_- (and therefore k_+). We estimate this error

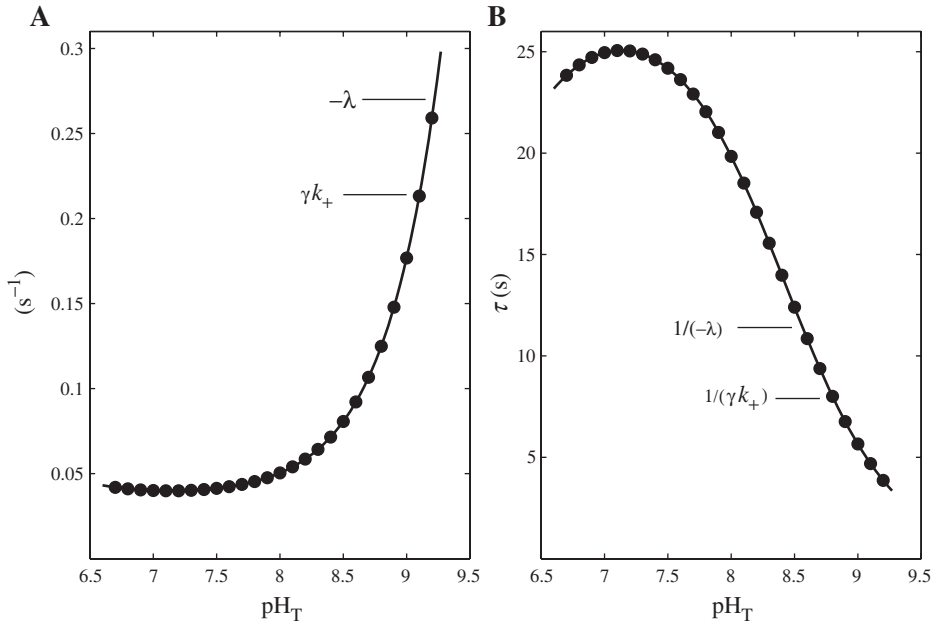

Fig. 6. Comparison of γk_+ (dots), with k_+ calculated as for Fig. 5, and the eigenvalues λ of the carbonate system (solid line) described in Section 3.4 at 25 °C at a salinity of 35 between pH 7 and 9. A compares γk_+ with λ while B illustrates the inverse of these values, which are the relaxation times τ of the carbonate system upon disturbance.

to be up to 50% depending on temperature, pH and MIMS setup.

3.4. Theoretical remarks on $k_+ = k_{+1} + k_{+4}[OH^-]$

It can be shown that the conversion of CO_2 to HCO_3^- on time scales monitored by the MIMS (i.e., seconds) is given by the slowest process, which is characterized by the relaxation time τ:

$$\tau = -\frac{1}{\lambda} \tag{30}$$

$$\lambda = -\frac{1}{2}\left(k_- + k_+ + \bar{k}_- + \bar{k}_+\right) + \frac{1}{2}\sqrt{\left(k_- + k_+ - \bar{k}_- - \bar{k}_+\right)^2 + 4k_-\bar{k}_-}\quad , \tag{31}$$

with $k_- = k_{-1}[H^+] + k_{-4}$, $k_+ = k_{+1} + k_{+4}[OH^-]$, $\bar{k}_- = k_{-5}^{H^+} + k_{+5}^{OH^-}[OH^-]$, and $\bar{k}_+ = k_{+5}^{H^+}[H^+] + k_{-5}^{OH^-}$. Because of the rapid interconversion of HCO_3^- and CO_3^{2-}, the exact solution for $[CO_2](t)$ at constant pH can excellently be approximated by Eq. (16), with

$$\tau \approx \frac{1}{\gamma k_+}. \tag{32}$$

as shown in Fig. 6B.

In summary, if the pH buffer is able to keep the pH constant upon disturbance in the carbonate system, the rate constants for the CO_2 to HCO_3^- interconversion, k_+ and k_-, can be calculated as $k_+ = k_{+1} + k_{+4}[OH^-]$ and $k_- = k_+ K_1^*$ (see Table 1 for details on the rate constants).

4. Summary and conclusions

Mass spectrometric and ^{14}C disequilibrium techniques are widely used to assess modes and efficiencies of inorganic carbon acquisition in marine phytoplankton (Badger et al., 1994; Espie and Colman, 1986). These methods rely on the exact knowledge of the rate constants for the CO_2 to HCO_3^- interconversion reaction, which depend on pH, temperature and salinity. In this study, a method is presented for measuring these rate constants, known as k_+ and k_-, by means of membrane inlet mass spectrometry (MIMS). For the two pH buffers tested (HEPES and BICINE) it was shown that measured rate constants are in good agreement with calculated values for k_+ and k_- in a pH range of 7 to 8.5 and at temperatures from 10 to 25 °C. Moreover, it was shown that the method proposed previously to determine the CO_2 to HCO_3^- interconversion rate constants tends to significantly underestimate them. Therefore, it is recommended that in future applications k_+ and k_- are measured or calculated as described above.

Acknowledgements

We thank K.-U. Richter for technical assistance and A. Körtzinger for vital discussions regarding the carbonate system. This work was funded by the Deutsche Forschungsgemeinschaft (DFG) project #TH 744/2-1.

Appendix A

The reaction scheme for the hydration of carbon dioxide can be formulated as (cf. Eigen et al. (1961))

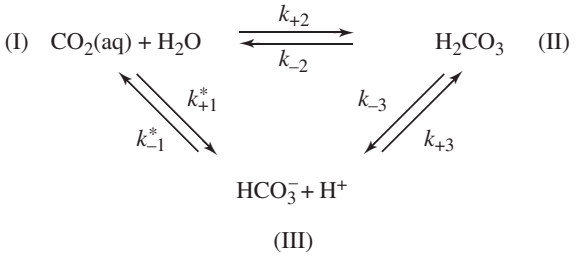

in which aqueous carbon dioxide (CO_2(aq)) is either hydrated in the transition of (I) to (III) or via H_2CO_3 in the transition of (I) to (II) to (III). The overall hydration and dehydration reaction as measured by Johnson (1982) is then given as

$$CO_2 + H_2O \underset{k_{-1}}{\overset{k_{+1}}{\rightleftharpoons}} H^+ + HCO_3^- \tag{A-1}$$

with CO_2 denoting the sum of CO_2(aq) and H_2CO_3, and k_{+1} and k_{-1} being the effective rate constants. As the reaction between carbonic acid and bicarbonate (II)⇋(III) is diffusion-controlled, it is practically instantaneous and equilibrium can be assumed as

$$[H^+]\left[HCO_3^-\right] = K^*_{H_2CO_3}[H_2CO_3] \tag{A-2}$$

with $K^*_{H_2CO_3}$ being the acidity constant of true carbonic acid. Hence, k_{+1} and k_{-1} of the overall hydration/dehydration reaction are given by

$$k_{+1}: = k^*_{+1} + k_{+2} \tag{A-3}$$

and

$$k_{-1}: = k^*_{-1} + \frac{k_{-2}}{K^*_{H_2CO_3}} \tag{A-4}$$

While the hydration/dehydration reaction is dominant at low pH, at high pH the reaction via hydroxylation is favored as

$$CO_2 + OH^- \underset{k_{-4}}{\overset{k_{+4}}{\rightleftharpoons}} HCO_3^- \qquad (A-5)$$

The combination of the hydration/dehydration and the hydroxylation reaction gives the overall interconversion reaction of CO_2 to HCO_3^- and vice versa as

$$H_2O + CO_2 \underset{k_-}{\overset{k_+}{\rightleftharpoons}} HCO_3^- + H^+ \qquad (A-6)$$

with

$$k_+ : = k_{+1} + k_{+4}[OH^-] \qquad (A-7)$$

and

$$k_- : = k_{-1}[H^+] + k_{-4} \qquad (A-8)$$

Note that the overall reaction (Eq. (A-6)) must not be confused with that given Eq. (A-1) as it incorporates also the hydroxylation pathway.

References

Badger, M.R., Palmqvist, K., Yu, J.-W., 1994. Measurement of CO_2 and HCO_3^- fluxes in cyanobacteria and microalgae during steady-state photosynthesis. Physiol. Plant. 90, 529–536.

Beynon, R.J., Easterby, J.S., 1996. Buffer Solutions: The Basics. Oxford University Press.

Burkhardt, S., Amoroso, G., Riebesell, U., Sültemeyer, D., 2001. CO_2 and HCO_3^- uptake in marine diatoms acclimated to different CO_2 concentrations. Limnol. Oceanogr. 46, 1378–1391.

Cooper, T.G., Filmer, D., Wishnick, M., Lane, M.D., 1969. The active species of "CO_2" utilized by riboluse diphosphate carboxylase. J. Biol. Chem. 244, 1081–1083.

Davies, C.W., 1962. Ion Association. Butterworths.

DOE, 1994. Handbook of methods for the analysis of the various parameters of the carbon dioxide system in seawater, version 2A. In: Dickson, A.G., Goyet, C. (Eds.), ORNL/CDIAC-74.

Eigen, M., 1964. Proton transfer, acid–base catalysis, and enzymatic hydrolysis. Angew. Chem., Int. Ed. Engl. 3, 1–19.

Eigen, M., Kustin, K., Maass, G., 1961. Die Geschwindigkeit der Hydratation von SO_2 in wässriger Lösung. Z. Phys. Chem. N.F. 30, 130–136.

Espie, G.S., Colman, B., 1986. Inorganic carbon uptake during photosynthesis: I. A theoretical analysis using the isotope disequilibrium technique. Plant. Physiol. 80, 863–869.

Field, C.B., Behrenfeld, M.J., Randerson, J.T., Falkowski, P., 1998. Primary production of the biosphere: integrating terrestrial and oceanic components. Science 281, 237–240.

Good, N.E., Winter, W., Conolly, T.N., Izawa, S., Singh, R., 1966. Hydrogen ion buffers for biological research. Biochemistry 5, 467–477.

Houghton, J.T., Meira Fiho, L.G., Bruce, J., Lee, H., Callander, B.A., Haites, E., Harris, N., Maskell, K. (Eds.), Climate Change 1994, Ch. Radiative Forcing of Climate Change and an Evaluation of the IPCC IS92 Emission Scenario. Cambridge Univ. Press, Cambridge.

Johnson, K.S., 1982. Carbon dioxide hydration and dehydration kinetics in seawater. Limnol. Oceanogr. 27, 849–855.

Moré, J.J., 1977. The Levenberg–Marquardt algorithm: implementation and theory. In: Watson, G.A. (Ed.), Numerical Analysis, Lecture Notes in Mathematics, vol. 630. Springer, pp. 105–116.

Rost, B., Riebesell, U., Burkhardt, S., Sültemeyer, D., 2003. Carbon acquisition of bloom-forming marine phytoplankton. Limnol. Oceanogr., 55–67.

Rost, B., Richter, K.-U., Riebesell, U., Hansen, P.J., in press. Inorganic carbon acquisition in red-tide dinoflagellates. Plant Cell Environ. doi:10.1111/j.1365-3040.2005.01450.x.

Roy, R.N., Roy, L.N., Lawson, M., Vogel, K.M., Porter-Moore, C., Pearson, T., Good, C.E., Millero, F.J., Cambel, D.J., 1993. Determination of the ionization constants of carbonic acid in seawater in salinities 5 to 45 and temperatures 0 to 45 °C. Mar. Chem. 44, 249–267.

Sabine, C.L., Feely, R.A., Gruber, N., Key, R.M., Lee, K., Bullister, J.L., Wanninkhof, R., Wong, C.S., Wallace, D.W.E., Tilbrook, B., Millero, F.J., Peng, T.-H., Kozyr, A., Ono, T., Rios, A.F., 2004. The oceanic sink for anthropogenic CO_2. Science 305, 367–371.

Shampine, L.F., Reichelt, M.W., 1997. The matlab ODE suite. SIAM J. Sci. Comput. 18, 1–22.

Sültemeyer, D., Price, G.D., Yu, J.-W., Badger, M.R., 1995. Characterization of carbon dioxide and bicarbonate transport during steady-state photosynthesis in the marine cyanobacterium Synechococcus strain PCC7002. Planta 197, 597–607.

Thoms, S., Pahlow, M., Wolf-Gladrow, D., 2001. Concentrating mechanisms in chloroplasts of eukaryotic algae. J. Theor. Biol. 208, 295–313.

Zeebe, R.E., Wolf-Gladrow, D., 2001. CO_2 in seawater: equilibrium, kinetics, isotopes. Vol. 65 of Elsevier Oceanography Series. Elsevier.

Zeebe, R.E., Wolf-Gladrow, D.A., Jansen, H., 1999. On the time required to establish chemical and isotopic equilibrium in the carbon dioxide system in seawater. Mar. Chem. 65, 135–153.